Morphogenesis-Inspired Two-Dimensional Electrowetting in Droplet Networks

Joyce El-Beyrouthy¹, Michelle Makhoul-Mansour^{1,2}, Jesse Gulle¹, Eric Freeman^{1*}

¹School of Environmental, Civil, Agricultural, and Mechanical Engineering, University of Georgia, Athens, GA, USA.

²College of Engineering, University of Tennessee Knoxville, Knoxville, TN, USA.

*ecfreema@uga.edu

Abstract

Living tissues dynamically reshape their internal cellular structures through carefully regulated cell-to-cell interactions during morphogenesis. These cellular rearrangement events, such as cell sorting and mutual tissue spreading, have been explained using the differential adhesion hypothesis, which describes the sorting of cells through their adhesive interactions with their neighbors. In this manuscript we explore a simplified form of differential adhesion within a bioinspired lipid-stabilized emulsion approximating cellular tissues. The artificial cellular tissues are created as a collection of aqueous droplets adhered together in a network of lipid membranes. Since this abstraction of the tissue does not retain the ability to locally vary the adhesion of the interfaces through biological mechanisms, instead we employ electrowetting with offsets generated by spatial variations in lipid compositions to capture a simple form of bioelectric control over the tissue characteristics. This is accomplished by first conducting experiments on electrowetting in droplet networks, next creating a model for describing electrowetting in collections of adhered droplets, then validating the model against the experimental measurements. This work demonstrates how the distribution of voltage within a droplet network may be tuned through lipid composition then used to shape directional contraction of the adhered structure using two-dimensional electrowetting events. Predictions from this model were used to explore the governing mechanics for complex electrowetting events in networks, including directional contraction and the formation of new interfaces.

Keywords

Electrowetting, droplet interface bilayers, morphogenesis, adaptive structures

Introduction and Motivation

Living tissues are assembled from collections of cells that are capable of emergent behaviors and collective outputs. The hierarchical, interwoven structure of the cells within the tissue determines the overall functionality and form. Consequently, patterning and differentiation of the individual cells is a crucial step during morphogenesis. Morphogenesis is controlled through biomechanical processes [1, 2] and biochemical pathways [3-5]. The biomechanical processes, where forces are generated to drive cellular reconfiguration, is commonly explained through the differential adhesion hypothesis (DAH) [6-10].

The DAH is a thermodynamic framework that predicts cellular self-assembly and the global development of tissue patterns through variable and heterogeneous adhesive properties between neighboring cells. More favorable interfaces expand while less favorable interfaces contract until equilibrium is reached at a local minimum of the interfacial energy. Adjusting the energetic cost per interface produces dynamic rearrangements of the cellular structures as they seek new equilibriums. This is accomplished through a complex multitude of cell-cell interactions, including actomyosin contractions and cadherin-cadherin interactions [1, 6]. These mechanisms modulate the adhesion of the cell-cell interfaces, and produce variable compaction, wherein the tissue draws closer together. According to the DAH, given a starting random mixture of two distinct cell types, the final equilibrium configuration of the tissue is achieved when the two cell types spontaneously sort, and a sphere of the more cohesive cells (those with a higher surface tension) is formed within a spheroid of the less cohesive cells (those with a lower surface tension) [11]. While this is not a complete description of tissue reorganization [8, 12, 13], it still provides a framework for their exploration.

Models predicting DAH mechanics typically employ an energetics-based approach, similar to approaches for immiscible liquid mixtures [2, 14-16]. Values are provided for the cost of formation (or tensions, γ), for cell-cell contacts (γ_{cc}), and cell-medium/matrix contacts (γ_{cm}) [16], with additional terms added for pressures [14], area elasticity [7], and contractility [17] among others. The adhered geometry is determined by calculating the motion of

the vertices through the summed contribution of each of these terms, seeking the equilibrium configuration or balance of the interfaces. This equilibrium may be described by the Young-Dupre tension balance, where the equilibrium contact angle between two cells is governed by the balance of their cell-cell and cell-medium tensions as shown in Figure 1.a. Varying the ratio of these two tensions produces compaction, where the cells are drawn closer together as the favorability of their adhesion increases. This allows for changes in the shape of the tissue [15, 16] and the relative dimensions of the cell-cell interfaces. This may be expanded to larger tissues with similar principles as shown in Figure 1.b.

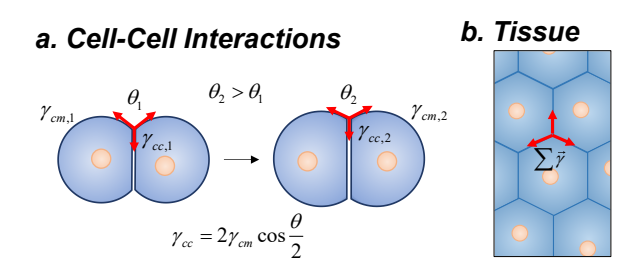


Figure 1—a) Compaction occurs in living tissues when the tension of the cell-cell interfaces becomes more favorable relative to the cell-medium interface, allowing the cells to draw closer together and balancing the tensions at the vertices. b) These principles may be applied towards larger tissues, allowing for a description of shape changes during morphogenesis through varying local tensions.

Morphogenesis has been investigated experimentally using emulsive models, modifying the adhesion strength within an oil-in-water emulsion and monitoring droplet reconfiguration events [18]. In this work we explore a similar concept through tension-driven adaptation of water-in-oil droplets (droplet interface bilayers, or DIBs) [19-22] as shown in Figure 2. These are collections of aqueous droplets dispersed in an oil medium with dissolved phospholipids in either or both phases. The lipids spontaneously self-assemble at the surface of the aqueous droplets, acting as a surfactant. When the lipid-coated droplets are brought into contact, their surfaces join together and adhere to form lipid bilayers expelling the residual oil during this process. The structures of these materials are described through the balance of their tensions and bear a striking resemblance to the emulsive approximation of living tissues described in Figure 1, both in their equilibrium structure [23, 24] as well as their functionality [25-27]. Here the cell-cell interfaces (γ_{cc}) are replaced by lipid bilayers (γ_b), and the cell-medium interfaces (γ_{cm}) are replaced by lipid monolayers (γ_m). The tensions associated with DIBs [28] are typically higher than living tissues [15], consequently a network of DIBs may be loosely described as a stiff tissue [17].

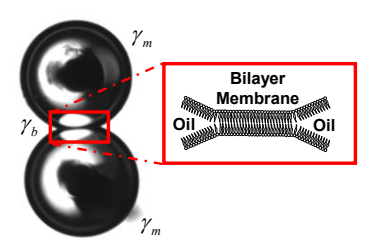


Figure 2 – The Droplet Interface Bilayer (DIB) technique forms lipid bilayer membranes at the intersections of lipid-coated aqueous droplets submerged in an oil reservoir. The resulting structures are similar to the abstraction living tissues and are governed by similar balances of interfacial tensions.

Rearrangement in living tissues is achieved through varying the properties of the individual interfaces [16]. In DIBs, this spatial variations of the tensions is difficult to achieve since the interfacial properties are primarily dictated by the composition of the aqueous and continuous phases [23, 28, 29], and there are limited methods for tuning interfacial tensions on an interface-by-interface basis after the network is formed through changes in the membrane composition. As an alternative to controlling the membrane characteristics, living cells also maintain electrical potential difference between their cytoplasm and the surrounding extracellular environment [30]. This potential provides a summary of the cell state [31]. While the full extent of this potential over the cellular capabilities is currently under examination,

the modulation of this membrane potential through the manipulation of membranous properties has been shown to generate significant mutations both in functionality and form of the tissue [32]. This suggests that the membrane potential provides a regulating influence over morphogenesis in living tissues. Taking this as inspiration, we use a distribution of voltages across the DIB networks to control the adhesion between the droplets.

These distributions of voltages in DIBs produce electrowetting, where the voltage across the membrane temporarily increases the favorability of formation, promoting wetting and drawing the droplets together [33-35]. This electrowetting phenomena provides a means for temporarily adjusting the tension across the joined droplet-droplet interfaces. While vastly simplified from its natural origins, this approach couples the adhesion strength of the droplets with a bioelectric distribution of voltages within the collection of droplets. This results in a voltage-driven adjustment of the droplet-droplet interfaces that is inspired by morphogenesis while simpler in scope and implementation.

Electrowetting in DIBs has been primarily studied in single membrane systems; however, 2D and even 3D structures of DIBs may be built with multiple membranes [23, 36]. Electrowetting within networks may provide more complex phenomena as the distribution of voltages within the network is variable, divided across the collection of membranes between the source and ground electrodes [27, 37]. The distribution of voltages within DIB networks has been successfully modeled in the past using nodal voltage analysis [37-39]. The individual membrane response to electrowetting has been studied and modeled in detail as well [28, 33, 40]; but wetting and voltage distributions in DIBs containing more than one membrane have not been studied at this time.

This is explored here through a multiphysics model combining the electrical and mechanical properties of adhered droplet structures. While models exist for simulating the mechanics of DIB tissues through their energetics [24] and models exist for predicting the distribution of voltages within the tissue [37, 39], a model that predicts how electrowetting will shape the adhered DIB structure is necessary to highlight how voltage-driven contraction events may be used to approximate aspects of morphogenesis within a DIB tissue. These DIB tissues have been proposed as functional droplet networks [36, 41, 42], neuromorphic or computing materials [40, 43, 44], tailored membranous architectures [45, 46], and platforms for exploring cell-cell signaling and gene circuitry [5, 47, 48]. Enhancing DIBs with the ability to reshape and adapt through bioelectric principles will augment these existing applications by providing them with a form of cell plasticity [49].

Materials and Methods

Experimental Methodology and Materials

Lipid Solutions

Lipids-in-droplets are prepared by first dissolving 250 mM of potassium chloride (KCl, ≥99.1%—Sigma-Aldrich) with 10 mM MOPS (of 3-(N-Morpholino) propane sulfonic acid (MOPS, ≥99.5%—Sigma-Aldrich) in DI water. DPhPC and 1,2-di-O-phytanyl-sn-glycero-3-phosphocholine (DOPhPC) are purchased from Avanti Polar Lipids, dissolved in chloroform. The desired amount of the chloroform is evaporated through a two-step process: argon gas exposure followed by placing the vial in a vacuum chamber overnight to produce the desired lipid films. The resulting dry lipid films are then hydrated with the buffer solution leading to a final 2 mg/mL concentration.

Once the lipids are dispersed, at least 6 freeze—thaw cycles (freeze at -20°C, and thaw at room temperature) are performed to ensured proper distribution of liposomes. Before usage, the needed volume is extracted and sonicated using a bath sonicator (Elma Ultrasonics) for 20 minutes followed by probe tip sonicator (Q55 QSONICA, LLC) for cyclical periods of 2 minutes at 30 W (ON then OFF) until the solution is clear, typically requiring five cycles.

Network Assembly

Circular (2.5 cm diameter 0.3 cm depth) polyurethane wells are adhered to a glass slide and used as the oil reservoir for membrane network assembly. Glass capillaries (1 mm diameter) are sharpened to fine tips, filled with the desired lipid solutions, and connected to a microinjector and micromanipulator for droplet deposition. Once the droplets are deposited the network is formed by bringing the droplets into contact. The formation and characterization of the network is then observed through microscopy and electrophysiology as will be discussed in the following paragraphs.

Electrophysiology

Electrodes are prepared by submerging 250 μm diameter silver wires (Goodfellow) in sodium hypochlorite (NaClO) solution for several minutes forming silver/silver-chloride (Ag/Ag-Cl) electrodes. The electrodes are then threaded through glass microcapillaries filled with a 40% w:v polyethylene glycol dimethacrylate (PEG-DMA 1000) hydrogel (Polysciences) containing Irgacure 2959 (Sigma Aldrich) as the photoinitiator, and the hydrogel is then cured in place through UV-LED exposure (Thorlabs) to fix the wires in place. The wire tips are then dipped in agarose hydrogel (2.5% w:v low EEO, Sigma-Aldrich) allowing for improved adhesion of the droplets to the electrodes. The input electrode is connected to the headstage of the Axopatch amplifier, while the other one is connected to the ground. Electrical noise is reduced by grounding the equipment and by placing the membrane network and both electrodes within a Faraday cage. Measurements are conducted using an Axopatch 200B patch-clamp amplifier operating in voltage-clamp mode connected back to a Digidata 1440 (Molecular Devices). Waveforms are provided using a function generator supplying a sinusoidal voltage (10 mV, 40 Hz) to measure the membrane capacitance combined with a series of step functions provided by a MyDAQ (Labview) operated using MATLAB scripts to provide the DC voltages for electrowetting. The resulting current as a function of time and voltage is then post-processed in MATLAB to produce plots of membrane capacitance. These plots of membrane capacitance may then be compared to simulated cases.

Microscopy

An inverted microscope (Leica DMI3000B) with a CCD camera (Leica DFC365 FX) and software (Leica LASX) is utilized to observe the formed network and responses to the applied voltage. This light microscopy allows for clear images of the network and its rearrangements.

Modeling Methodology

We propose calculating the adhered structure of the droplet network using a method similar to Brakke *et.al* in the Surface Evolver model [50, 51] through minimization of interfacial energies. Here this approach is merged with a particle-based approach wherein each droplet is capable of motion and the interfacial dimensions are calculated by the distance between the droplet centers then coupled with an electrical overlay to incorporate electrowetting from the experiments. This approach is similar to a model produced by Bahadur and Garimella [52] and extended to include multiple interfaces and the ability to separate and reconnect the droplets. While excellent models exist for replicating the mechanics of droplet-based tissues [25, 53], this model simulates the mechanical-electrical coupling by calculating the droplet-droplet forces as functions of interfacial tensions and transmembrane potentials and allows for simulation inputs taken directly from experimental measurements.

Droplet Mechanics Model

The equilibrium configuration of the droplets is based on the minimization of the interfacial energy within the adhered configuration, assuming negligible gravitational influences on the droplet shape. The base tensions for each interface (bilayer and monolayer) are assumed to be constant and are taken from literature values or determined experimentally when necessary. Any transient increases in these tension values due to distortion of the interfaces and changes in areaper-lipid are assumed to occur at a faster timescale than the droplet motion and are therefore negligible in these simulations. Consequently, the energy per droplet may be written as the areas multiplied by their respective tensions (Equation (1)):

$$E_{drop} = \gamma_m A_m + \frac{1}{2} \gamma_b^{app} A_b \tag{1}$$

where the energy associated with a single drop is equal to the monolayer tension (γ_m) multiplied by the monolayer area (A_m) and half the apparent bilayer tension (γ_m^{app}) multiplied by the bilayer area (A_b) (Figure 3), as the bilayer area is shared between two droplets. The apparent bilayer tension (γ_m^{app}) is used since this bilayer tension may be adjusted from the base tension value through electrowetting as described in the next section [28, 52, 54, 55].

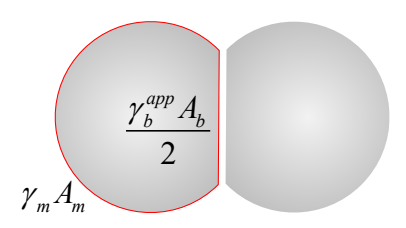


Figure 3 – Each droplet within the DIB possesses an interfacial energy that may be estimated by multiplying the area devoted to each interface (monolayer, bilayer) by their respective cost of formation.

Microdroplets free of external perturbations or gravitational influences adopt a spherical shape to minimize their interfacial energetics [50], consequently each droplet is described using spherical cap approximations as outlined in the **Supplementary Information** and in previous research [56]. Once a mutually agreeable configuration is found through an iterative approach, the total energy for each droplet is calculated by multiplying the interfacial tensions by their resolved respective areas.

Electrical Network Model

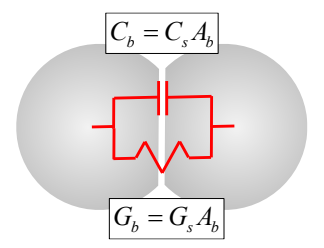


Figure 4 – Each membrane is electrically approximated as a capacitor in parallel with a $G\Omega$ resistor (when no transmembrane channels are incorporated). Values for the capacitance and conductance are obtained by multiplying the area of the adhered interface by standard values for the specific capacitance and specific conductance of lipid bilayers.

The membranes between the droplets may be approximated as a capacitor and resistor in parallel as shown in Figure 4, following the classic Hodgkin-Huxley approximation of the lipid membrane [57]. For this study it is assumed that the resistance of the droplet interiors is negligible [24, 38]. This means that each droplet is represented as a single node with a uniform voltage Vi, separated from neighboring nodes by the electrical approximation of the membranes formed between their interfaces.

The electrical properties of each interface are scaled from the membrane areas, using values for the specific capacitance C_s and specific conductance G_s . The specific conductance is assumed to remain constant in this work and is typically in the G Ω range. The specific capacitance C_s may be determined as a function of the voltage drop across the membrane shown in Equation (2), where α is the electrocompression coefficient and the resting specific capacitance $C_{s,\theta}$ [54].

$$C_s = C_{s,0} \left(1 + \alpha V_b^2 \right) \tag{2}$$

Once the properties of the interfaces are resolved through the areas and transmembrane voltages, the current i across each membrane (here formed between droplets 1 and 2) may be written as a function of the adjacent droplet voltages that comprise the membrane (Equation (3)):

$$i = C_b \left(\frac{dV_2}{dt} - \frac{dV_1}{dt} \right) + \frac{dC_b}{dt} \left(V_2 - V_1 \right) + G_b \left(V_2 - V_1 \right)$$
(3)

where C_b is the net membrane capacitance and G_b is the net membrane conductance, obtained by multiplying the interfacial area by their associated coefficients. The change in capacitance with respect to time (dC_b/dt) is approximated from the history of each interface using a backwards finite difference scheme. Using nodal voltage analysis and Kirchoff's current law (KCL), the summed current entering or leaving each droplet is set to zero (Equation (4)).

$$[C_b] \left\{ \frac{dV}{dt} \right\} + \left(\left[\frac{dC_b}{dt} \right] + \left[G_b \right] \right) \left\{ V \right\} = 0$$

$$\left\{ \frac{dV}{dt} \right\} = - \left[C_b \right]^{-1} \left(\left(\left[\frac{dC_b}{dt} \right] + \left[G_b \right] \right) \left\{ V \right\} \right)$$

$$(4)$$

The derivative of the voltage within each droplet with respect to time may be isolated by taking the inverse of the capacitance matrix $[C_b]$ and multiplying by the remaining terms on the right-hand side of the equation. This produces a system of differential equations for the voltage within each droplet that is dependent on the voltages of their surrounding neighbors. This creates a system of n differential equations for the voltage, where n is the number of droplets.

The capacitance and conductance matrices are originally assumed to be $n \times n$ in dimension – this assumes that an electrical connection exists between every possible droplet pair. Any rows and columns where the interfacial area between the droplets is zero are removed from the system of equations, but they have the capacity for reformation based on the droplet trajectories. Boundary conditions are applied for the source and ground droplets to produce the solution, adding current to the source droplet to simulate charging and setting the ground droplet to a constant potential [38].

Asymmetric Electrowetting

The electrical and mechanical models are combined through the reduction of apparent interfacial tension due to electrowetting. The bilayer tension for each interface is adjusted by Equation (5):

$$\gamma_b^{app} = \gamma_{b,0} - \frac{1}{2} C_s V_b^2 \tag{5}$$

The value V_b represents the voltage across the bilayer, or the transmembrane voltage. This is defined by the difference between the voltage in the two adjacent droplets, combined with the internal field produced by differences in lipid leaflets. Asymmetric membranes are simply constructed in DIBs by varying the lipid composition dissolved within adjacent droplets [58], forming the membrane from two different lipid monolayers. Since each lipid has an electrostatic profile containing dipole (φ_d) and surface potentials (φ_s) linked to the structure of the lipids and their solvation [59-62], an offset is produced within the membrane when these profiles are no longer symmetric. When electrodes are introduced this asymmetry produces an offset in the minimum electric field across the membrane. This shifts the electrowetting phenomena, producing minimal membrane dimensions when the internal offset voltage (ΔV_{asymm}) is compensated through an externally supplied voltage rather than 0 mV as shown in Figure 5.c [63-66].

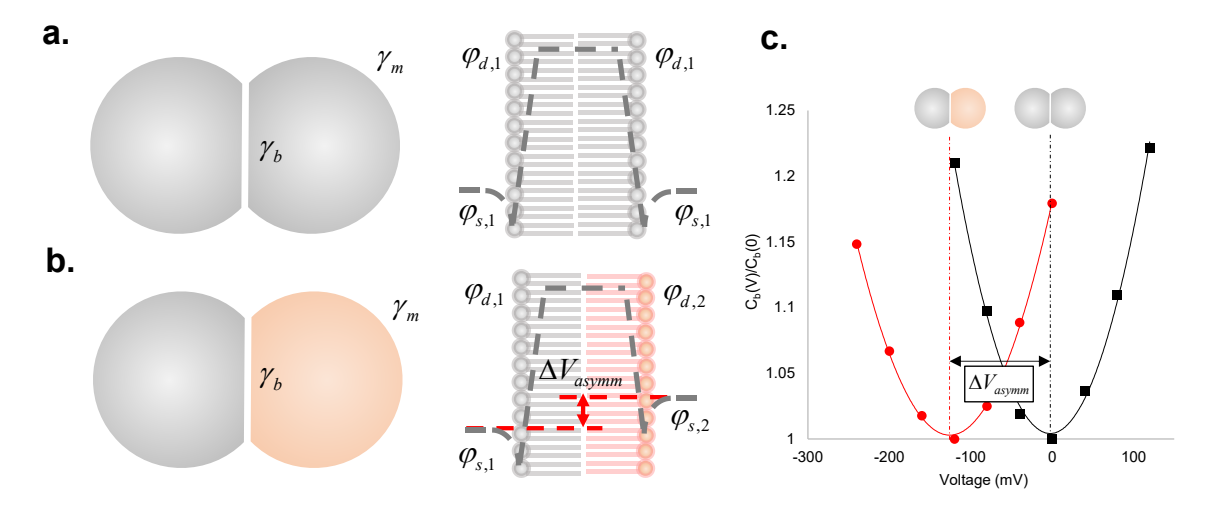


Figure 5 – Droplet Interface Bilayers (DIBs) are formed between two adhered lipid-coated droplets, and possess a monolayer (droplet-medium) and bilayer (droplet-droplet) interface. The bilayers at the interface possess an electrostatic profile dependent

on the lipid type. a) Typically, these electrostatic profiles are symmetric and the boundary potentials are equal. b) However, asymmetric membranes formed from two droplets containing different lipids generate an offset voltage ΔV_{asymm} . This offset may be either a function of differences between the dipole potential or the surface potentials of the leaflets and is related to the leaflet structure and solvation [42]. c) This offset is then reflected in the electrowetting response of the membrane, where the minimum membrane area (C_b) occurs when the offset voltage is compensated, adapted from [66].

To simulate asymmetry, each droplet entity is assigned an internal offset voltage dependent on the lipids present within the droplet, selecting 1,2-diphytanoyl-sn-glycero-3-phosphocholine (DPhPC) as the default reference (offset = 0 mV). The difference between these offset voltages between the droplets that comprise each membrane is taken into account when describing the voltage across the membrane (Equation (6)).

$$V_b = (V_i - V_j) + \underbrace{(V_{l,i} - V_{l,j})}_{\Delta V_{asymm}} \tag{6}$$

While asymmetric droplet interface bilayers (DIBs) have been characterized extensively [40, 59, 63, 67], most studies on asymmetric DIB membranes have involved single interfaces. Typically, electrodes are present in both droplets, clamping the boundaries at either side of the membrane to the prescribed voltage from the electrophysiology apparatus and charging the asymmetric membrane. One example in the literature without electrodes present reported that the asymmetry does still enhance transport through charged membranes [67], but at a lowered rate. This suggests that asymmetric membranes are not necessarily charged in isolation, and that additional mechanisms are necessary. Any exchange of charge between the droplets will alter the transmembrane potential. These exchanges will occur due to either ion transport across the membranes or through current provided by the bounding electrodes short circuiting the membranes. To best capture this, we set the initial potential within each droplet to the asymmetric potential. This produces a voltage difference that will drive current across the membranes, and gradually corrects the initial offset, but the internal field used in electrowetting (Equation (5)) is zero prior to droplet-droplet exchanges.

Droplet Trajectories

To estimate the forces on each droplet, the droplets' locations are perturbed in the x, y, and z directions and the change in the energy per droplet is calculated. These changes are used to estimate the gradient of the internal energy for each droplet using finite central difference approximations (Equation (7)), and the negative gradient of the energy produces the force on each droplet [52, 53] associated with capillary effects.

$$\vec{F}_{E,drop} \approx -\vec{\nabla} E_{drop} \approx -\left\{ \begin{aligned} &\frac{E_{drop} \left(x + \Delta x, y, z \right) - E_{drop} \left(x - \Delta x, y, z \right)}{2 \Delta x} \\ &\frac{E_{drop} \left(x, y + \Delta y, z \right) - E_{drop} \left(x, y - \Delta y, z \right)}{2 \Delta y} \\ &\frac{E_{drop} \left(x, y, z + \Delta z \right) - E_{drop} \left(x, y, z - \Delta z \right)}{2 \Delta z} \end{aligned} \right\}$$
(7)

This force is then combined with a single damping force dependent on the current droplet velocity defined by a viscous damping coefficient β . While we recognize that there are multiple damping forces present involving droplet wetting and motion [68], this damping value is simply added to replicate the observed behavior of the droplets.

Finally, we assume that the inertial effects of the droplets are negligible. The masses of the droplets are exceedingly small (nanoliter volumes), and they will rapidly reach their terminal velocities within the oil [69]. Consequently, the velocity is directly taken from the necessary drag force for counterbalancing the forces estimated from the previous equation (Equation (8)). This greatly reduces the necessary computational time for integration. Friction between the droplets is assumed negligible since the lipids are able to glide laterally across the surfaces of the droplets [70].

$$\sum_{i} \vec{F}_{drop} = 0 = \vec{F}_{E,drop} - \vec{v}\beta$$

$$\vec{v} = \frac{\vec{F}_{E,drop}}{\beta}$$
(8)

The result is a collection of differential equations, scaling with the number of droplets present. Future work may include changing the contents of the droplets [39] and their volumes associated with osmotic effects [25]. The differential equations are integrated using Runge-Kutta methods, specifically Dormand-Prince as described in **Supplementary Information**. Results are then post-processed for comparison against experiments and plotted in MATLAB for visualization where desired as collections of overlapping spheres. Tracked variables include the voltage within each droplet, transmembrane potentials, current supplied across the electrodes, and membrane dimensions.

Model Inputs

Simulation input values (summarized in Table 1) are based on water droplets containing DPhPC lipids dispersed in buffer solutions and deposited in a varying continuous phase. Values for the monolayer and bilayer tension for DPhPC are obtained from previous experimental works when available or measured as discussed in the SI [28, 33]. The damping coefficient which serves to regulate droplet motion and vibrations is selected to best match experimental behaviors. Values for the specific capacitance and specific conductance taken from multiple studies [28, 33, 38, 54, 71, 72]. Inputs for any simulations used to produce the figures are provided as supplementary files.

Result and Discussion

Validation Against Experiments

Table 1 – Simulation Parameters and Sources for DPhPC DIBs in Various Solvents

Variable	Tetradecane	Source	Hexadecane	Source	Hexadecane:Silicone Oil AR20 (2:1)	Source	Hexadecane:Silicone Oil AR20 (1:1)	Source
Monolayer Tension (γ_m)	1.32 mN/m	Measured (see SI)	1.14 mN/m	Literature Values [28, 33]	1.10 mN/m	Literature Value [56]	1.06 mN/m	Literature Value [56]
Bilayer Tension (%)	2.56 mN/m	Measured (see SI)	2.07 mN/m	Literature Values [28, 33]	1.85 mN/m	Literature Value [56]	1.59 mN/m	Literature Value [56]
Damping (β)	~20*10 ⁻³ Ns/m	Variable, Estimated	~20*10 ⁻³ Ns/m	Variable, Estimated	~20*10 ⁻³ Ns/m	Variable, Estimated	~20*10 ⁻³ Ns/m	Variable, Estimated
Electrocompression (α)	5.36 1/V ²	Literature Value [33]	1.75 1/V ²	Literature Value [33]	N/A	Not used	N/A	Not used
Specific Capacitance $(C_{s\theta})$	0.538 μF/cm ²	Measured (see SI)	0.652 μF/cm ²	Literature Values [28, 33, 54, 71]	N/A	Not used	N/A	Not used
Specific Conductance (G_s)	5 nS/cm ²	~GΩ Range [37, 38, 72]	5 nS/cm ²	~GΩ Range [37, 38, 72]	N/A	Not used	N/A	Not used

All inputs for validation against experimental cases are taken from the literature or measured as summarized in Table 1, aside from the damping factor β , which is estimated using comparisons against experimental results in the single membrane cases. The final two columns with varying oils are used to simulate reconfiguration through externally supplied forces (Figure 9), and did not involve the application of voltages across the membranes, so values for the electrical characteristics of the membranes are not necessary. For each of the following cases, the input files used to generate these results may be found in the **Supplementary Information**.

Single Membrane Comparisons

First the behavior of a droplet pair forming a single DIB in hexadecane is studied. Two cases are presented – one symmetric, and one asymmetric as shown in Figure 6. The voltage offset in the asymmetric case is set to +135 mV to match the expected difference between DPhPC and DOPhPC, measured experimentally in similar DIBs in hexadecane from previous works [63, 73, 74]. Electrowetting behaviors for single DIBs are well-documented in the literature and serve as calibration cases [52]. A series of step voltages are applied from +135 mV to -135 mV both experimentally

and within the model to demonstrate maximum contraction and separation of the two droplets, and demonstrate nullification of the asymmetric membrane offset in response to a DC voltage. The simulated capacitance is processed for both cases and compared against experimental data as shown in Figure 6. All inputs are taken from Table 1 for hexadecane, with the droplet sizes initially estimated from the images shown and tuned to provide an equivalent matching initial capacitance at 0 mV. As expected, the symmetric membrane exhibits the same wetting behavior with ± 1.35 mV, while the asymmetric membrane exhibits a maximum capacitance at 135 mV and minimum capacitance at ± 1.35 mV, where the intramembrane asymmetry is compensated [66]. The changes in capacitance represent contraction or separation of the droplets, producing changes in the dimensions of their adhered interface. The growth and decay of the membrane area are matched by varying the damping coefficient β which will be used in the remaining simulations. Symmetric droplet pairs produce contraction for both positive and negative voltages, while the asymmetric cases produce contraction or separation dependent on the signal polarity. In both cases the droplet motions are defined by the vectors formed between the droplet centers.

The model reasonably captures the experimentally measured trends. Electrowetting is reproduced in the model by droplet motion generated through changes in the interfacial tensions using Equation (7). Initial drifts in the predicted capacitances from the model are associated with the droplets moving to their equilibrium positions from their initial coordinates. The severe contraction exhibited for asymmetric membranes at positive voltages may be partially inhibited by the presence of the electrodes themselves, which are not present in the equations for the model. Furthermore, the inputs in Table 1 are taken from symmetric DPhPC-DPhPC cases rather than asymmetric membranes. However, the model is still able to capture the variable contraction produced through membrane asymmetry and may be used to explore behavior in networks.

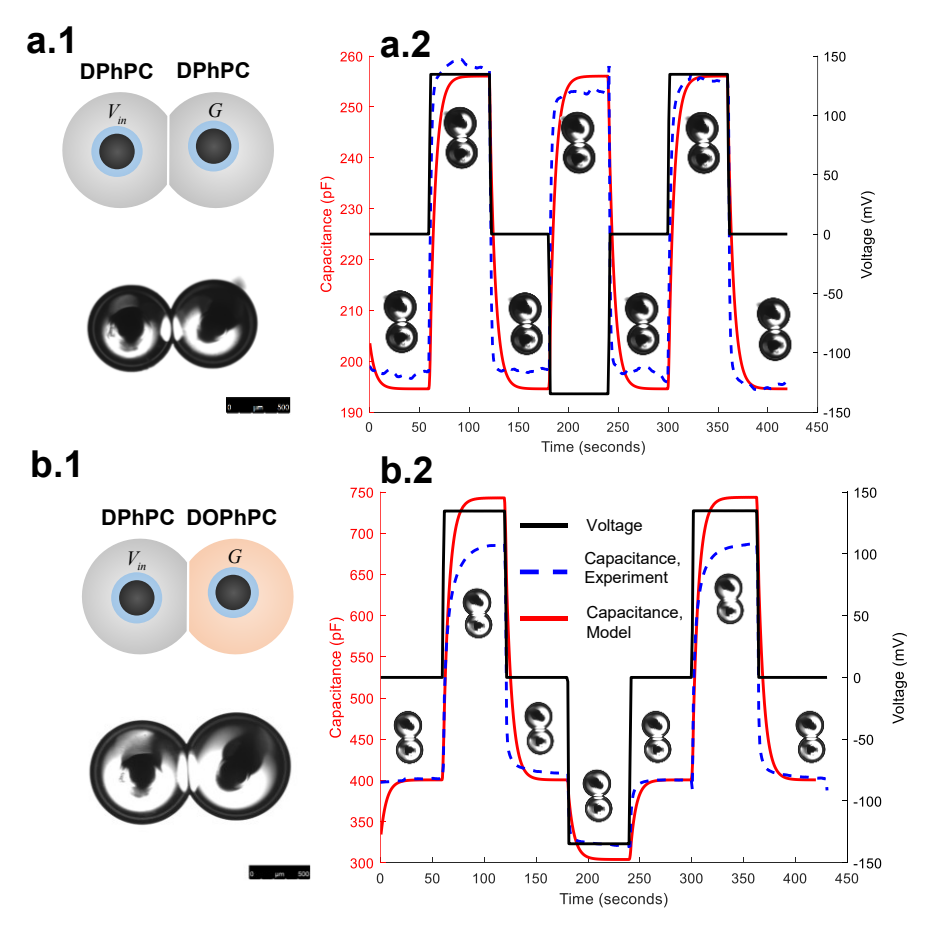


Figure 6 - A single DIB is formed in hexadecane. Panel a) shows a symmetric membrane with comparisons between the experimentally measured capacitance and predicted capacitance. The droplets show even contraction for both negative and

positive voltage steps. Panel b) shows an asymmetric membrane with the same comparisons. Here the droplet pair exhibits contraction with positive voltages and expansion with a negative voltage. Scale bars are 500 µm.

Multiple Membrane Comparisons and Variable Contraction Events

Next, we explore larger networks of droplets, demonstrating two-dimensional electrowetting. In these cases, the phenomena are not as straight forward as single membranes, as the distribution of voltages across multiple membranes is dependent on the distribution of membrane area and vice versa. The case investigated involves two parallel chains of droplets containing two membranes each as shown in Figure 7. The top row of droplets contain DPhPC, and the lower row of droplets contain DOPhPC. This produces symmetric vertical membranes and asymmetric horizonal membranes. The voltage applied between the source and ground electrodes is then split across these membranes.

A similar voltage function is applied experimentally, doubling the applied voltage from 135 mV to 270 mV to distribute the voltages in a similar fashion across the membranes. The total capacitance of the network is plotted with respect to time for both the experimental case and the simulated case. Notably the model captures the dependence on the polarity of the signal. The response to a positive voltage input is amplified, while the response to a negative voltage input is minimized as the offsets generated by the asymmetric membranes cancel out the supplied voltage.

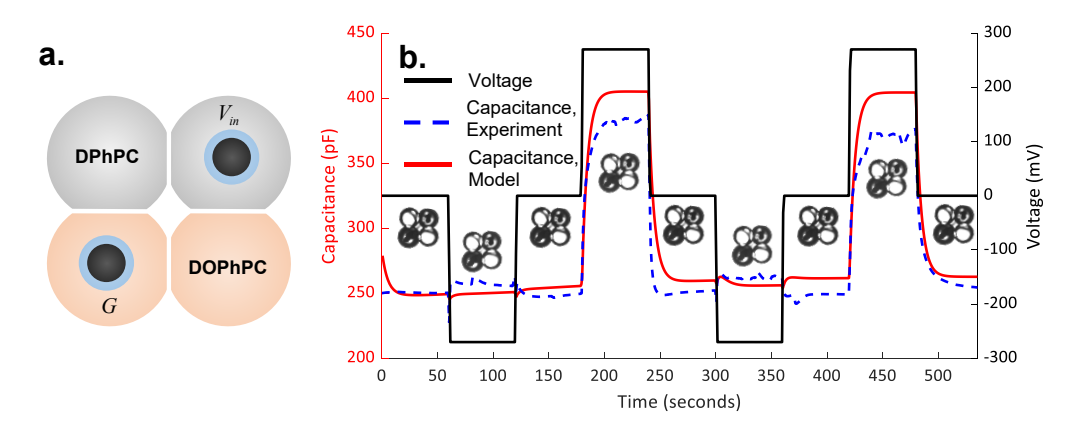


Figure 7 – Networks of asymmetric droplets in hexadecane exhibit directional contraction dependent on the polarity of the applied voltage. A positive potential produces contraction, where the offsets contribute to the transmembrane potentials, and a negative potential produces reconfiguration, where symmetric membranes expand and asymmetric membranes shrink producing a negligible change in the measured net capacitance.

The shape of the droplet network is changed in response to the voltage (**Supplementary Video 1**). The negative voltages produce simultaneous wetting and dewetting of the interfaces in the network, resulting in a negligible change in the net capacitance. Since the droplet pairs are simultaneously contracting and separating, this produces a change in the network shape through electrowetting in multiple dimensions. The droplets move along the vectors defined between their centers, and in this case these vectors are constructed in multiple dimensions leading to changes in the network shape, approximating morphogenesis in a simple fashion. The peaks are underpredicted similarly to the two-droplet case, likely due to the presence of the electrodes or differences in the properties of asymmetric DPhPC-DOPhPC membranes from the measured symmetric characteristics in Table 1. For each of these comparisons slight changes in the supplied tensions γ_m and γ_b may be used to ensure a match between the predictions and experimental results; however, we have opted to present the results for a consistent single collection of experimentally-obtained inputs (Table 1) for simplicity.

The asymmetry in the network's electrowetting response to the applied voltage is regulated by a combination of the maximum offset voltage provided by the asymmetric lipid membranes coupled with the magnitude of the electrowetting energy compared to the energy of adhesion of the membrane. To explore how this may be magnified, we propose a reduction in tensions to values similar to those observed in natural tissues, setting γ_m to 0.3 mN/m and γ_0 to 0.58 mN/m, similar to the ranges of tensions reported for the ectoderm of a cell [15]. It may be feasible to further amplify the voltage offset presented by the lipid asymmetry through surface adsorption [66], but the 135 mV offset provided by the DPhPC-DOPhPC pairing is currently the largest observed offset in the literature for lipid-based DIB

systems. The remaining characteristics are left identical to the network presented in Figure 7. A triangular wave voltage (5 mHz, 270 mV) is simulated between the source and ground electrode, and the x and y dimensions of the network (total width and total height) are recorded and normalized against the resting dimensions of the network at 0 mV and plotted with respect to voltage in Figure 8. These results are then plotted against the baseline values for tensions in hexadecane used in the previous simulations for comparison.

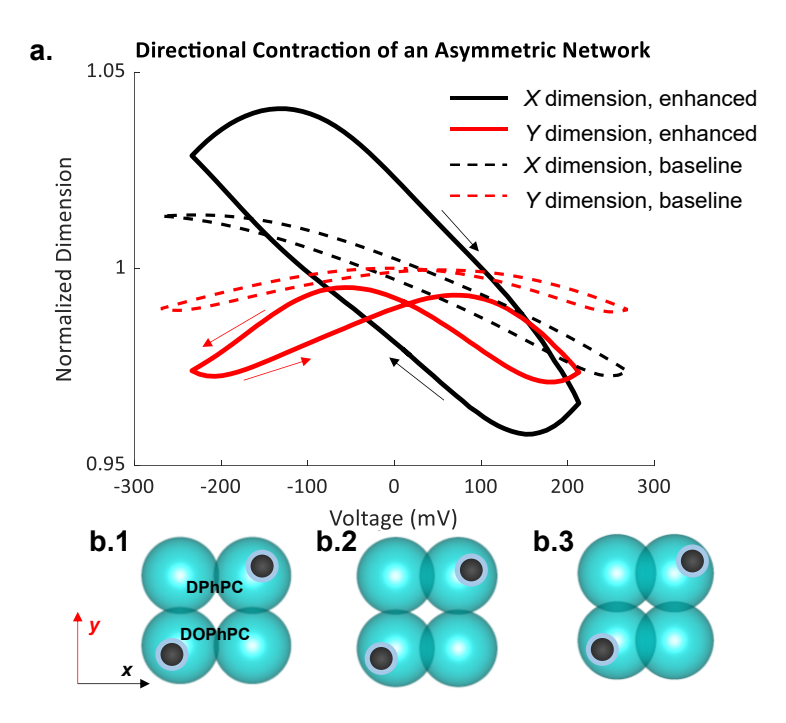


Figure 8 – a) Simulated electrowetting under both amplified ectoderm conditions and standard DIB conditions reported as the total network width (X dimension) and height (Y dimension). The results show directional contraction and even expansion in the X dimension of the network with a negative voltage. Simulated images of the droplet arrangement and apparent radii are provided for b.1) -270 mV, b.2) 0 mV, and b.3) 270 mV with the ectoderm conditions.

From this figure we see that the network contracts in both dimensions with a positive voltage, corresponding to the maximum capacitance reached in Figure 7. However, the negative voltage produces a combined contraction in the y dimension and expansion in the x dimension, producing directional electrowetting dependent on the signal polarity. Furthermore, the model captures aspects of the classic hysteresis behavior observed in brain-inspired DIB electrowetting systems [40, 64]. While this is not the emphasis of this work, it is encouraging to see the expected hysteresis trends produced as the membrane dimensions lag behind the voltage signal.

Separation and Reconfiguration of the DIB Tissue

A strength of the selected modeling approach is the ability to capture droplet separation and the formation of new interfaces, as the model defines the membrane interfaces by the overlap between adjacent droplets which often change across the droplet trajectories. We use this feature to investigate two cases: the first is taken from a recent work on ferrofluid-enabled magnetic reconfiguration [56] and the second proposes how to accomplish similar processes at cellularly-relevant scales through simultaneous electrowetting of multiple interfaces.

Magnetic nanoparticles suspended in aqueous solutions (ferrofluids) have been used to create motor droplets within the droplet-based tissues, manipulating the adhered droplets through magnetic forces [42, 46, 56, 75]. Similar concepts have been used to assess tissue stiffness and drive rearrangements through ferrofluid droplets in living tissues [76, 77]. This was used recently to demonstrate intercalation events in DIB networks by anchoring select droplets and pulling others, separating and reforming the interfacial membranes as shown in Figure 9. These rearrangements were then used to rearrange the ionically conductive pathways within the printed droplets [56]. It was noted during the experiments that an increasing adhesive strength between the droplets enhanced the stability of the network at the expense of requiring greater forces to separate the membranes. As the droplets approached cellularly-relevant

dimensions the amount of force necessary for separation was no longer feasible using the available collection of electromagnets and compatible ferrofluids due to the stiffness of DIB tissues [56].

To explore these observations using our model, we examined the necessary force for droplet separation within a four-droplet network as a function of the interfacial properties. We set the damping value β (Equation (8)) to $1/100^{th}$ of the values selected in Table 1 to ensure that the droplets quickly reach equilibrium in response to an external force with minimal response lag. We then specified an external body force in the x direction on one of the droplets for the simulated ferrofluid droplet, beginning at 0 N then linearly increasing with time. The force necessary to separate the simulated ferrofluid droplet and the anchored droplet, initiating reconfiguration, is recorded and plotted as a function of the energy of adhesion, calculated as $\Delta F = 2\gamma_m - \gamma_b$ [33] using the values in Table 1 and plotted in Figure 9.c. The structure of the model permits the simulation of the droplets separating and reforming the membrane in the ferrofluid-assisted T1 event, and a linear relationship between the energy of adhesion of the membranes and the necessary body force to separate the membranes is produced. A video of the experiment may be seen in **Supplementary Video 2**.

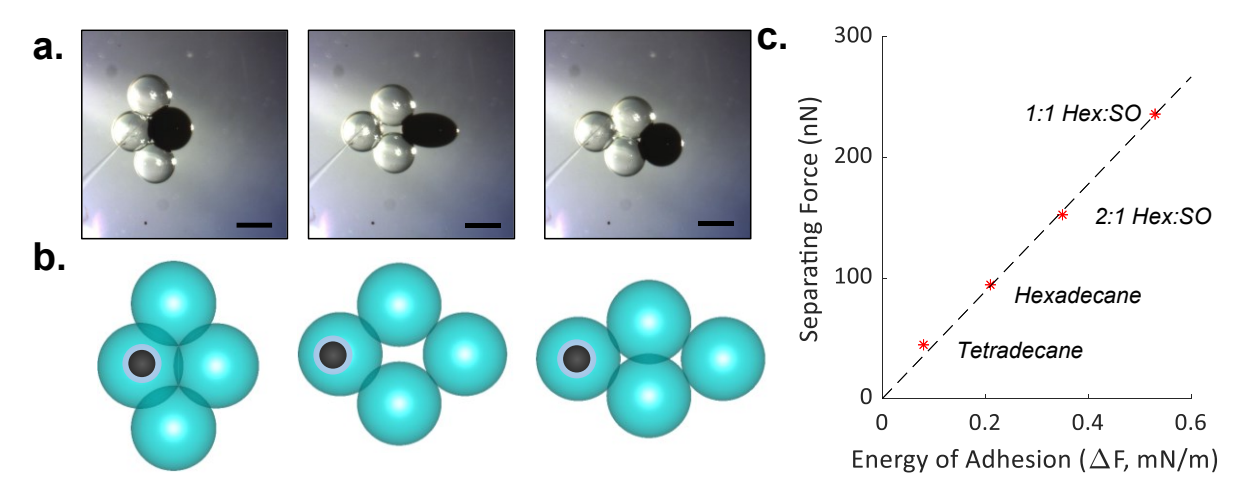


Figure 9 – Simulating intercalation events using the model. a) In a previous work, a ferrofluid droplet is used to separate then reform the lipid membranes, adapted from [56] b) This was recreated in the model by fixing one droplet then gradually applying a force to the rightmost droplet as shown in the simulated reconfiguration. The simulation was repeated with varying compositions listed in Table 1 and the resulting force for separation exhibited a near-linear trend with respect to the adhesion energy $\Delta F = 2\gamma_m - \gamma_b$ as shown in panel c. Scale bars are 500 μ m.

The observed reduced effectiveness at lower droplet volumes is due to the scaling involved with magnetic forces — the maximum force generated per motor droplet scales with the volume of the ferrofluid [56], while the force necessary for separation scales with the interfacial areas, producing a threshold for separation that increases linearly with the inverse of the droplet radii. Consequently, a voltage-driven rearrangement is preferable as it directly manipulates the bilayer apparent tension (Equation (5)). A four-droplet cluster is created with the droplets originally positioned to create two separate adhered paths between the electrodes, establishing a gap between the central droplets as shown in Figure 10. Upon the application of a voltage step, the central droplets are pulled towards both droplets on the electrodes simultaneously, drawing them together. Once the droplets come into contact, a new "bridge" membrane is formed between the droplets. This membrane remains in place after the voltage is removed, demonstrating the ability to change the metastable configuration of the network using a voltage signal, reproducing bioelectric control over morphogenesis in a simple platform. The experiment and simulation were conducted in tetradecane (Table 1), and an experimental video may be seen in **Supplementary Video 3**.

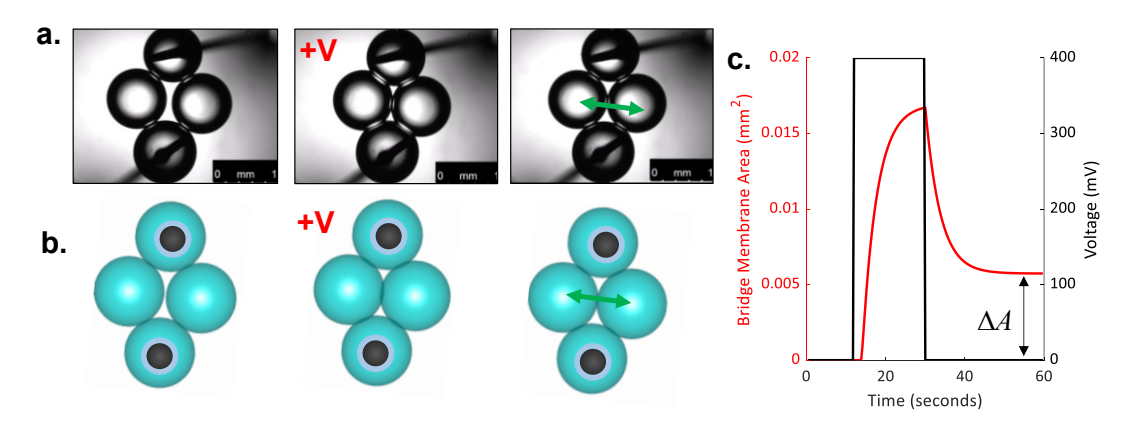


Figure 10 – A bridge membrane may be formed using a voltage signal through contraction of the droplets as shown here in tetradecane. a) This was conducted in the laboratory, then b) simulated in the model as shown by the post-processed droplet locations and overlaps defining the interfaces. In both cases, a bridge membrane is formed that persists c) after the voltage step is removed as shown here as the simulated interfacial area of the newly formed membrane. Scale bars are 1 mm.

Conclusions

In this manuscript we develop and test a coupled electrical-mechanical model for networks of adhered functional droplets to explore voltage-driven contraction and reconfiguration events in collections of adhered droplets as inspired by morphogenesis. This model is built on the principle of minimizing interfacial energies in emulsive systems combined with an electrical approximation of the underlying membranes, and allows for predictions of coupled mechanical and electrical effects in droplet-based synthetic tissues. While previous research efforts successfully modeled the electrical properties of these materials as networks of capacitors and resistors, this manuscript describes the first model to link these electrical elements to the geometries of the adhered droplets and use them to successfully explore electrowetting in networks containing multiple interfaces. The model was successfully compared against experimental results and showcased how electrowetting in DIBs may be recreated through simple models using experimentally-derived coefficients.

Using this model we illustrate how networks of droplets exhibit multi-directional electrowetting in response to voltage signals. Furthermore, we demonstrate how to use tailored asymmetric membranes to redistribute these voltages and produce polarity-sensitive contraction of the droplet networks. These phenomena may be used to accomplish basic voltage-driven contraction of larger droplet networks, exhibiting changing shapes and shifts in the wetted interfacial area in a fashion inspired by the capabilities of living tissues to sort and organize through varying interfacial characteristics governed in part through a bioelectric distribution.

Author Contributions

J.B. developed the original concept, conducted the experiments, and developed the manuscript, M.M.M. assisted with concept development, sample preparation, analysis, and reviewed the manuscript, J.G. conducted asymmetric network experiments and reviewed the manuscript, E.F. assisted with concept development, developed the model, executed the simulations for model validation, and developed the manuscript.

Supplementary Information

Additional details on the modeling methodology are provided in the Supplementary Information, along with a tutorial on use of the model. The model may be downloaded along with input scripts that produced the results in the figures from https://github.com/ecfreema/DropSim_Bioinsp-Biomim. Three videos are provided of the observed experimental behaviors.

Data Accessibility

The model and input files necessary for each figure are provided as supplementary information. Additional experimental traces and data are available from the corresponding author upon request.

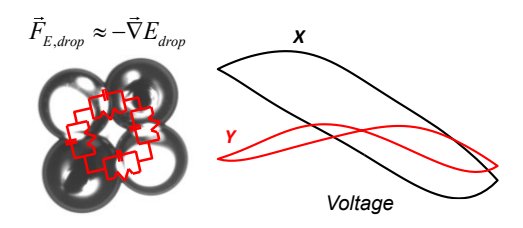
Conflicts of Interest

There are no conflicts to declare.

Acknowledgements

The authors graciously acknowledge financial support from NSF grant #1537410 and grant #1903965.

Table of Contents



Shape-shifting droplet networks approximating morphogenesis are produced through coordinated electrowetting events and captured in a novel multiphysics model.

References

- 1. Wickström, S.A. and C.M. Niessen, *Cell adhesion and mechanics as drivers of tissue organization and differentiation: local cues for large scale organization.* Current opinion in cell biology, 2018. **54**: p. 89-97.
- 2. Winklbauer, R., *Cell adhesion strength from cortical tension—an integration of concepts.* Journal of Cell Science, 2015. **128**(20): p. 3687-3693.
- 3. Mitalipov, S. and D. Wolf, *Totipotency, pluripotency and nuclear reprogramming*, in *Engineering of stem cells*. 2009, Springer. p. 185-199.
- 4. Nakano, T., M. Moore, A. Enomoto, and T. Suda, *Molecular communication technology as a biological ICT*, in *Biological functions for information and communication technologies*. 2011, Springer. p. 49-86.
- 5. Dupin, A., L. Aufinger, I. Styazhkin, F. Rothfischer, B.K. Kaufmann, S. Schwarz, N. Galensowske, H. Clausen-Schaumann, and F.C. Simmel, *Synthetic cell-based materials extract positional information from morphogen gradients*. Science Advances, 2022. **8**(14): p. eabl9228.
- 6. Amack, J.D. and M.L. Manning, *Knowing the boundaries: extending the differential adhesion hypothesis in embryonic cell sorting.* Science, 2012. **338**(6104): p. 212-215.
- 7. Glazier, J.A. and F. Graner, Simulation of the differential adhesion driven rearrangement of biological cells. Physical Review E, 1993. **47**(3): p. 2128.
- 8. Steinberg, M.S., *Differential adhesion in morphogenesis: a modern view*. Current opinion in genetics & development, 2007. **17**(4): p. 281-286.
- 9. Steinberg, M.S., Adhesion-guided multicellular assembly: a commentary upon the postulates, real and imagined, of the differential adhesion hypothesis, with special attention to computer simulations of cell sorting. Journal of theoretical biology, 1975. **55**(2): p. 431-443.
- 10. Steinberg, M.S., Reconstruction of tissues by dissociated cells. Science, 1963. 141(3579): p. 401-408.
- 11. Jakab, K., B. Damon, F. Marga, O. Doaga, V. Mironov, I. Kosztin, R. Markwald, and G. Forgacs, *Relating cell and tissue mechanics: implications and applications*. Developmental dynamics: an official publication of the American Association of Anatomists, 2008. **237**(9): p. 2438-49.
- 12. Harris, A.K., *Is cell sorting caused by differences in the work of intercellular adhesion? A critique of the Steinberg hypothesis.* Journal of theoretical biology, 1976. **61**(2): p. 267-285.
- 13. Nishizawa, K., S.-Z. Lin, C. Chardès, J.-F. Rupprecht, and P.-F. Lenne, *Two-point optical manipulation reveals mechanosensitive remodeling of cell-cell contacts in vivo.* bioRxiv, 2022.
- 14. Alt, S., P. Ganguly, and G. Salbreux, *Vertex models: from cell mechanics to tissue morphogenesis*. Philosophical Transactions of the Royal Society B: Biological Sciences, 2017. **372**(1720): p. 20150520.
- David, R., O. Luu, E.W. Damm, J.W. Wen, M. Nagel, and R. Winklbauer, *Tissue cohesion and the mechanics of cell rearrangement*. Development, 2014. **141**(19): p. 3672-3682.
- 16. Turlier, H. and J.-L. Maître. *Mechanics of tissue compaction*. in *Seminars in cell & developmental biology*. 2015. Elsevier.

- 17. Tetley, R.J. and Y. Mao, *The same but different: cell intercalation as a driver of tissue deformation and fluidity.* Philosophical Transactions of the Royal Society B: Biological Sciences, 2018. **373**(1759): p. 20170328.
- 18. Golovkova, I., L. Montel, F. Pan, E. Wandersman, A.M. Prevost, T. Bertrand, and L.-L. Pontani, *Adhesion as a trigger of droplet polarization in flowing emulsions*. Soft Matter, 2021. **17**(14): p. 3820-3828.
- 19. Poulin, P. and J. Bibette, *Adhesion of water droplets in organic solvent*. Langmuir, 1998. **14**(22): p. 6341-6343.
- 20. Funakoshi, K., H. Suzuki, and S. Takeuchi, *Lipid bilayer formation by contacting monolayers in a microfluidic device for membrane protein analysis.* Anal Chem, 2006. **78**(24): p. 8169-74.
- 21. Bayley, H., B. Cronin, A. Heron, M.A. Holden, W.L. Hwang, R. Syeda, J. Thompson, and M. Wallace, *Droplet interface bilayers*. Mol Biosyst, 2008. **4**(12): p. 1191-208.
- 22. Booth, M., V.R. Schild, F. Downs, and H. Bayley, *Functional aqueous droplet networks*. Molecular BioSystems, 2017.
- 23. Alcinesio, A., O.J. Meacock, R.G. Allan, C. Monico, V.R. Schild, I. Cazimoglu, M.T. Cornall, R.K. Kumar, and H. Bayley, *Controlled packing and single-droplet resolution of 3D-printed functional synthetic tissues*. Nature Communications, 2020. **11**(1): p. 1-13.
- 24. Challita, E.J., M.M. Makhoul-Mansour, and E.C. Freeman, *Reconfiguring droplet interface bilayer networks through sacrificial membranes*. Biomicrofluidics, 2018. **12**(3): p. 034112.
- 25. Villar, G., A.D. Graham, and H. Bayley, A tissue-like printed material. Science, 2013. 340(6128): p. 48-52.
- 26. Zhou, L., A.C. Wolfes, Y. Li, D.C. Chan, H. Ko, F.G. Szele, and H. Bayley, *Lipid-Bilayer-Supported 3D Printing of Human Cerebral Cortex Cells Reveals Developmental Interactions*. Advanced Materials, 2020: p. 2002183.
- 27. Challita, E.J., J.S. Najem, R. Monroe, D.J. Leo, and E.C. Freeman, *Encapsulating Networks of Droplet Interface Bilayers in a Thermoreversible Organogel*. Scientific Reports, 2018. **8**(1): p. 6494.
- 28. Taylor, G.J., G.A. Venkatesan, C.P. Collier, and S.A. Sarles, *Direct in situ measurement of specific capacitance, monolayer tension, and bilayer tension in a droplet interface bilayer.* Soft Matter, 2015. **11**(38): p. 7592-605.
- 29. Venkatesan, G.A., J. Lee, A.B. Farimani, M. Heiranian, C.P. Collier, N.R. Aluru, and S.A. Sarles, *Adsorption kinetics dictate monolayer self-assembly for both lipid-in and lipid-out approaches to droplet interface bilayer formation*. Langmuir, 2015. **31**(47): p. 12883-12893.
- 30. Hille, B., *Ionic channels of excitable membranes*. Vol. 2. 1984: Sinauer associates Sunderland, MA.
- 31. Levin, M. and C.J. Martyniuk, *The bioelectric code: An ancient computational medium for dynamic control of growth and form.* Biosystems, 2018. **164**: p. 76-93.
- 32. Srivastava, P., A. Kane, C. Harrison, and M. Levin, *A meta-analysis of bioelectric data in cancer, embryogenesis, and regeneration.* Bioelectricity, 2021. **3**(1): p. 42-67.
- 33. El-Beyrouthy, J., M.M. Makhoul-Mansour, G. Taylor, S.A. Sarles, and E.C. Freeman, *A new approach for investigating the response of lipid membranes to electrocompression by coupling droplet mechanics and membrane biophysics*. Journal of the Royal Society Interface, 2019. **16**(161): p. 20190652.
- 34. Punnamaraju, S. and A.J. Steckl, *Voltage control of droplet interface bilayer lipid membrane dimensions*. Langmuir, 2011. **27**(2): p. 618-26.
- 35. Tamaddoni, N., G. Taylor, T. Hepburn, S.M. Kilbey, and S.A. Sarles, *Reversible, voltage-activated formation of biomimetic membranes between triblock copolymer-coated aqueous droplets in good solvents.* Soft Matter, 2016. **12**(23): p. 5096-5109.
- 36. Makhoul-Mansour, M.M. and E.C. Freeman, *Droplet-Based Membranous Soft Materials*. Langmuir, 2021.
- 37. Hwang, W.L., M.A. Holden, S. White, and H. Bayley, *Electrical behavior of droplet interface bilayer networks: experimental analysis and modeling*. Journal of the American Chemical Society, 2007. **129**(38): p. 11854-11864.
- 38. Creasy, M.A., E.C. Freeman, M.K. Philen, and D.J. Leo, *Deterministic model of biomolecular networks with stimuli-responsive properties*. Journal of Intelligent Material Systems and Structures, 2014: p. 1045389X14536004.
- 39. Freeman, E.C., A.B. Farimani, N.R. Aluru, and M.K. Philen, *Multiscale modeling of droplet interface bilayer membrane networks*. Biomicrofluidics, 2015. **9**(6): p. 064101.
- 40. Najem, J.S., M.S. Hasan, R.S. Williams, R.J. Weiss, G.S. Rose, G.J. Taylor, S.A. Sarles, and C.P. Collier, *Dynamical nonlinear memory capacitance in biomimetic membranes*. Nature communications, 2019. **10**(1): p. 1-11.

- 41. Holden, M.A., D. Needham, and H. Bayley, *Functional bionetworks from nanoliter water droplets*. J Am Chem Soc, 2007. **129**(27): p. 8650-5.
- 42. Downs, F.G., D.J. Lunn, M.J. Booth, J.B. Sauer, W.J. Ramsay, R.G. Klemperer, C.J. Hawker, and H. Bayley, *Multi-responsive hydrogel structures from patterned droplet networks*. Nature Chemistry, 2020. **12**(4): p. 363-371.
- 43. Najem, J.S., G.J. Taylor, R.J. Weiss, M.S. Hasan, G. Rose, C.D. Schuman, A. Belianinov, C.P. Collier, and S.A. Sarles, *Memristive ion channel-doped biomembranes as synaptic mimics*. ACS nano, 2018. **12**(5): p. 4702-4711.
- 44. Cazimoglu, I., M.J. Booth, and H. Bayley, *A lipid-based droplet processor for parallel chemical signals*. ACS nano, 2021. **15**(12): p. 20214-20224.
- 45. Elani, Y.S., XCI; Edel; JB; Law, RV; Ces, O, *Microfluidic generation of encapsulated droplet interface bilayer networks (multisomes) and their use as cell-like reactors.* Chemical Communications, 2016. **52**(35): p. 5961-5964.
- 46. Li, J., W.D. Jamieson, P. Dimitriou, W. Xu, P. Rohde, B. Martinac, M. Baker, B.W. Drinkwater, O.K. Castell, and D.A. Barrow, *Building programmable multicompartment artificial cells incorporating remotely activated protein channels using microfluidics and acoustic levitation*. Nature Communications, 2022. **13**(1): p. 1-12.
- 47. Aufinger, L. and F.C. Simmel, *Establishing communication between artificial cells*. Chemistry–A European Journal, 2019. **25**(55): p. 12659-12670.
- 48. Dupin, A. and F.C. Simmel, Signalling and differentiation in emulsion-based multi-compartmentalized in vitro gene circuits. Nature Chemistry, 2018: p. 1.
- 49. Theise, N. and D. Krause, *Toward a new paradigm of cell plasticity*. Leukemia, 2002. **16**(4): p. 542-548.
- 50. Berthier, J. and K.A. Brakke, *The physics of microdroplets*. 2012: John Wiley & Sons.
- 51. Brakke, K.A., *The Surface Evolver*. Experimental Mathematics, 1992. **1**(2): p. 141-165.
- 52. Bahadur, V. and S. Garimella, *An energy-based model for electrowetting-induced droplet actuation*. Journal of Micromechanics and Microengineering, 2006. **16**(8): p. 1494.
- 53. Zhang, T., D. Wan, J. Schwarz, and M. Bowick, *Shape-shifting droplet networks*. Physical Review Letters, 2016. **116**(10): p. 108301.
- 54. Gross, L.C., A.J. Heron, S.C. Baca, and M.I. Wallace, *Determining membrane capacitance by dynamic control of droplet interface bilayer area.* Langmuir, 2011. **27**(23): p. 14335-42.
- 55. Anklam, M., D. Saville, and R. Prud'Homme, *Disjoining Pressure and Film Tension in Comb— Graft Copolymer-Stabilized Oil Films*. Langmuir, 1999. **15**(21): p. 7299-7307.
- 56. Makhoul-Mansour, M.M., J.B. El-Beyrouthy, L. Mao, and E.C. Freeman, *Enhancing membrane-based soft materials with magnetic reconfiguration events*. Scientific Reports, 2022. **12**(1): p. 1-13.
- 57. Hodgkin, A.L., A.F. Huxley, and B. Katz, *Measurement of current-voltage relations in the membrane of the giant axon of Loligo*. The Journal of physiology, 1952. **116**(4): p. 424.
- 58. Hwang, W.L., M. Chen, B. Cronin, M.A. Holden, and H. Bayley, *Asymmetric droplet interface bilayers*. J Am Chem Soc, 2008. **130**(18): p. 5878-9.
- 59. Freeman, E.C., J.S. Najem, S. Sukharev, M.K. Philen, and D.J. Leo, *The mechanoelectrical response of droplet interface bilayer membranes*. Soft Matter, 2016. **12**(12): p. 3021-31.
- 60. Cevc, G., Membrane electrostatics. Biochim Biophys Acta, 1990. 1031(3): p. 311-82.
- 61. Ermakov, Y.A. and A. Nesterenko. *Boundary potential of lipid bilayers: methods and interpretations*. in *Journal of Physics: Conference Series*. 2017. IOP Publishing.
- 62. Clarke, R.J., *The dipole potential of phospholipid membranes and methods for its detection.* Advances in colloid and interface science, 2001. **89**: p. 263-281.
- 63. Taylor, G., M.-A. Nguyen, S. Koner, E. Freeman, C. Patrick Collier, and S.A. Sarles, *Electrophysiological interrogation of asymmetric droplet interface bilayers reveals surface-bound alamethic induces lipid flip-flop.* Biochimica et Biophysica Acta (BBA) Biomembranes, 2018.
- 64. Schoch, P., D.F. Sargent, and R. Schwyzer, Capacitance and Conductance as Tools for the Measurement of Asymmetric Surface-Potentials and Energy Barriers of Lipid Bilayer Membranes. Journal of Membrane Biology, 1979. **46**(1): p. 71-89.
- 65. Mosgaard, L.D., K.A. Zecchi, and T. Heimburg, *Mechano-capacitive properties of polarized membranes*. Soft Matter, 2015. **11**(40): p. 7899-910.
- 66. El-Beyrouthy, J., M.M. Makhoul-Mansour, and E.C. Freeman, *Studying the Mechanics of Membrane Permeabilization through Mechanoelectricity*. ACS Applied Materials & Interfaces, 2022.

- 67. Li, X., J. Huang, M.A. Holden, and M. Chen, *Peptide-Mediated Membrane Transport of Macromolecular Cargo Driven by Membrane Asymmetry*. Anal Chem, 2017.
- 68. Li, Y.-J., D. Echtermeyer, B.P. Cahill, and U. Pliquett, *Non-linearity and dynamics of low-voltage electrowetting and dewetting*. Physical Chemistry Chemical Physics, 2019. **21**(33): p. 18290-18299.
- 69. Durian, D.J., Foam mechanics at the bubble scale. Physical review letters, 1995. **75**(26): p. 4780.
- 70. Zhang, H. and H. Makse, *Jamming transition in emulsions and granular materials*. Physical Review E, 2005. **72**(1): p. 011301.
- 71. Beltramo, P.J., L. Scheidegger, and J. Vermant, *Towards realistic large area cell membrane mimics: Excluding oil, controlling composition and including ion channels.* Langmuir, 2018.
- 72. Creasy, M.A., *Bilayer Network Modeling*. 2011, Virginia Polytechnic Institute and State University.
- 73. Yasmann, A. and S. Sukharev, *Properties of diphytanoyl phospholipids at the air-water interface*. Langmuir, 2014.
- 74. Challita, E.J. and E.C. Freeman, *Hydrogel Microelectrodes for the Rapid, Reliable, and Repeatable Characterization of Lipid Membranes*. Langmuir, 2018.
- 75. Wauer, T., H. Gerlach, S. Mantri, J. Hill, H. Bayley, and K.T. Sapra, *Construction and manipulation of functional three-dimensional droplet networks*. ACS Nano, 2014. **8**(1): p. 771-9.
- 76. Mongera, A., M. Pochitaloff, H.J. Gustafson, G.A. Stooke-Vaughan, P. Rowghanian, S. Kim, and O. Campàs, *Mechanics of the cellular microenvironment as probed by cells in vivo during zebrafish presomitic mesoderm differentiation*. Nature Materials, 2022: p. 1-9.
- 77. Serwane, F., A. Mongera, P. Rowghanian, D.A. Kealhofer, A.A. Lucio, Z.M. Hockenbery, and O. Campàs, *In vivo quantification of spatially varying mechanical properties in developing tissues.* Nature methods, 2017. **14**(2): p. 181.